Supplementary Information

Real-time dynamics and cross-correlation gating spectroscopy of free-carrier Drude slow-light solitons

H. Zhou[1,4,*,†], S.-W. Huang[2,4,*,‡], X. Li[3,4], J. F. McMillan[4], C. Zhang[5], K. K. Y. Wong[5], M. Yu[6], G.-Q. Lo[6], D.-L. Kwong[6], K. Qiu[1], and C. W. Wong[2,4,§]

[1] Key Lab of Optical Fiber Sensing and Communication Networks, University of Electronic Science and Technology of China, Chengdu 611731, China.
[2] Mesoscopic Optics and Quantum Electronics Laboratory, University of California, Los Angeles, CA 90095, USA.
[3] College of Science, National University of Defense Technology, Changsha, Hunan 410073, China.
[4] Optical Nanostructures Laboratory, Columbia University, New York, NY 10027, USA.
[5] Department of Electrical and Electronic Engineering, The University of Hong Kong, Pokfulam Road, Hong Kong.
[6] Institute of Microelectronics, Agency for Science, Technology and Research, Science Park II, 117685, Singapore.

*equal contribution. E-mail: † zhouheng@uestc.edu.cn; ‡ swhuang@seas.ucla.edu;
§ cheewei.wong@ucla.edu.

I. Soliton perturbation under the influence of Drude free carrier dispersion

Here we conduct soliton perturbative analysis under the two-photon absorption induced Drude free carrier dispersion (FCD). Assuming the pulse width is much shorter than carrier lifetime and neglecting the propagation loss, the NLSE can be simplified and normalized by introducing the following dimensionless variables

$$u = \sqrt{\gamma_{eff} L_D} E \; ; \; \xi = \frac{z}{L_D} \; ; \; \tau = \frac{t}{T_0} \qquad (S1)$$

, where $L_D = \frac{T_0^2}{|\beta_2|}$ is the dispersion distance and T_0 is the pulse width.

The normalized NLSE can be obtained after some algebra as

$$i\frac{\partial u}{\partial \xi} + \frac{1}{2}\frac{\partial^2 u}{\partial \tau^2} + |u|^2 u = \kappa u \int_{-\infty}^{\tau} |u|^4 dt' \qquad (S2)$$

, where $\kappa = \frac{k_0 k_c |\beta_2| \beta_{TPA}}{2h\nu_0 A_0^2 \gamma_{eff}^2 T_0}$ is the dimensionless Drude FCD coefficient. Treating the FCD term as a perturbation (the assumption holds with limited pulse energies), the perturbed soliton solution of the NLSE can then be written as [SR1]

$$u(\xi,\tau) = A_m sech\big(A_m(\tau - q)\big) exp(-i\Omega\tau) \qquad (S3)$$

where A_m is the perturbed amplitude, q is the self-temporal shift, and Ω is the self-frequency shift. Using the variational method based on the Euler–Lagrange equation [SR1, SR2], the evolution of soliton parameters as functions of propagation can be determined by the following equations:

$$\frac{dA_m}{d\xi} = Re\left\{\int_{-\infty}^{\infty}\left(-i\kappa|u|^2\int_{-\infty}^{\tau}|u|^4dt'\right)d\tau\right\} \qquad (S4)$$

$$\frac{d\Omega}{d\xi} = -Im\left\{\int_{-\infty}^{\infty} tanh[A_m(\tau - q)]\left(-i\kappa|u|^2\int_{-\infty}^{\tau}|u|^4dt'\right)d\tau\right\} \qquad (S5)$$

$$\frac{dq}{d\xi} = -\Omega + \frac{1}{A_m}Re\left\{\int_{-\infty}^{\infty}(\tau - q)\left(-i\kappa|u|^2\int_{-\infty}^{\tau}|u|^4dt'\right)d\tau\right\} \qquad (S6)$$

As the integral in Eq. S4 is a pure imaginary number, we obtain the result that the soliton amplitude is not influenced by the Drude FCD. Without loss of generality, we set A_m = 1 and the right hand side of Eqs. S5-S6 can be integrated via Matlab symbolic algebra kit:

$$\frac{d\Omega}{d\xi} = \frac{8}{15}\kappa \qquad (S7)$$

$$\frac{dq}{d\xi} = -\Omega \qquad (S8)$$

The evolution of soliton self-frequency and temporal shift can be solved as:

$$\Delta\omega = \frac{\Omega}{T_0} = \frac{4}{15}\frac{k_0k_c\beta_{TPA}|\beta_2|^2}{h\nu_0A_0^2\gamma_{eff}^2T_0^4}z = \frac{4}{15}\frac{k_0k_c\beta_{TPA}}{h\nu_0A_0^2}z \qquad (S9)$$

$$\Delta t = qT_0 = -\frac{2}{15}\frac{k_0k_c\beta_{TPA}|\beta_2|^3}{h\nu_0A_0^2\gamma_{eff}^2T_0^4}z^2 = -\frac{2}{15}\frac{k_0k_c\beta_{TPA}|\beta_2|}{h\nu_0A_0^2}z^2 \qquad (S10)$$

On the right hand side of Eqs. S9 and S10, the fundamental soliton condition $N^2 = \frac{\gamma_{eff}T_0^2P_0}{|\beta_2|} = 1$ is applied.

II. Effect of linear loss on pulse propagation and spectrum broadening

The effect of linear loss on self-phase modulation is examined theoretically earlier in Ref. [SR3]. Figure S1 below shows the pulse propagation for different propagation along the photonic crystal for different linear losses: 10 dB/cm, 25 dB/cm, and 50 dB/cm. It is observed that linear loss does influence the pulse evolution in the silicon waveguide. In particular, as illustrated in Figure S1c

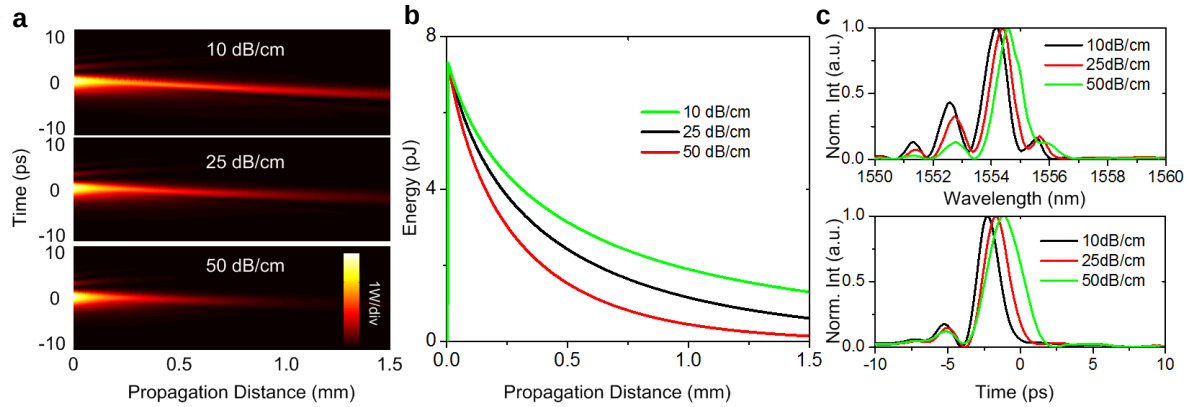

Figure S1 | Pulse propagating along photonic crystal for different linear losses. a, Evolution of the 1555 nm and 7.5 pJ input pulse; **b,** Pulse energy as a function of propagation distance. **c,** Output pulse waveforms and spectra under different waveguide losses.

below, for the 7.5 pJ pulse at 1555 nm, the spectrum-peak wavelength (temporal peak position) shifts 1.31 nm (-2.6 ps), 1.05 nm (-2.1 ps), and 0.94 nm (-1.6 ps) for 10 dB/cm, 25 dB/cm (the real device), 50 dB/cm loss respectively. In our measurements, the soliton number *N* is kept above 1, allowing the path-averaged solitons to broaden less [SR4].

Moreover, photonic crystal waveguides exhibit wavelength-dependent linear loss due to photonic bandgaps. Such limited transmission can influence the spectrum broadening of femtosecond pulses, as we discussed in Figure 4 of the main text. As shown in Figure S2, the measured transmission drops off fast at 1520 nm and 1566 nm. Correspondingly, the broadened pulse spectrum is subject to spectral filtering. This is confirmed by comparing the experimental measured spectrum (solid black line) and NLSE simulated spectrum without embedding the wavelength- dependent linear loss (dashed black line), as illustrated in Figure S2.

In addition, we also noticed that such wavelength-dependent linear loss would affect the accuracy of our discussion about Cherenkov radiation in Figure 4b of the main text. As exhibited in Figure S2, with the measured transmission included in NLSE, the Cherenkov radiation sideband is partially truncated and suppressed (solid green line, with 0% FCD), while the intact Cherenkov spectrum is notably higher and broader (dashed green line). Therefore, in Figure 4b of our main text, we replace the dispersive linear loss with a constant loss factor (13.0 dB/mm) so as to warrant accurate analysis on the FCD perturbation and resonant condition of Cherenkov radiation.

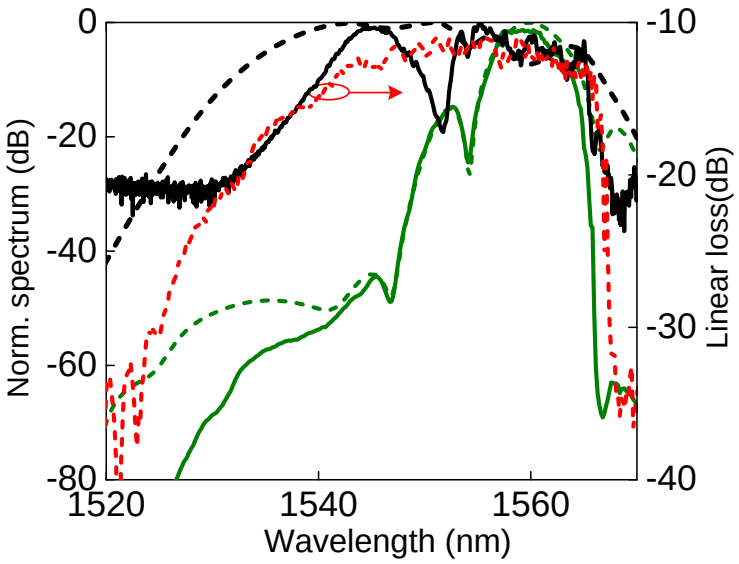

Figure S2 | Influence of wavelength-dependent linear loss of photonic crystal waveguide on femtosecond pulse spectrum broadening and Cherenkov radiation. The dashed red line to the right-Y axis shows the measured linear loss curve. The dashed black line shows the NLSE simulated broadened spectrum of 780 fs pulse without including the measured transmission curve, and the solid black line shows the experimental measured spectrum, illustrating clearly the impact of linear loss. Solid (dashed) green line shows the NLSE simulated Cherenkov radiation spectrum with (without) including the measured dispersive transmission, showing the effect of linear loss on the analysis of Cherenkov radiation.

III. Low dispersion-velocity dispersion waveguide via symmetric lattice shift

The photonic crystal waveguide used for Figure 4 in the main text is with specifically designed low group-velocity dispersion (GVD) regime via symmetric shift of air-holes in the third row apart from the single line defect. Such lattice shift can significantly modify the band structure of the planar photonic crystals, giving rise to the flexible group index and GVD of the defect-guided modes [SR5-SR7]. Figure S3a shows the optical micrograph of the chipset we used which contains groups of waveguide with a multitude of air-hole shift s (from 0 to 0.25a, a is the lattice constant). Using plane-wave expansion, we solved for the band structure and dispersion of the sample measured for Figure 4a (Group 2, Set 3, and Length 1, as marked in Figure S3a). The calculated photonic band structure is shown in Figure S3b, with the ninth band around 1550 nm (our measurement wavelengths). The inset of Figure S3b shows the resolved n_g and GVD curve from the ninth band. It

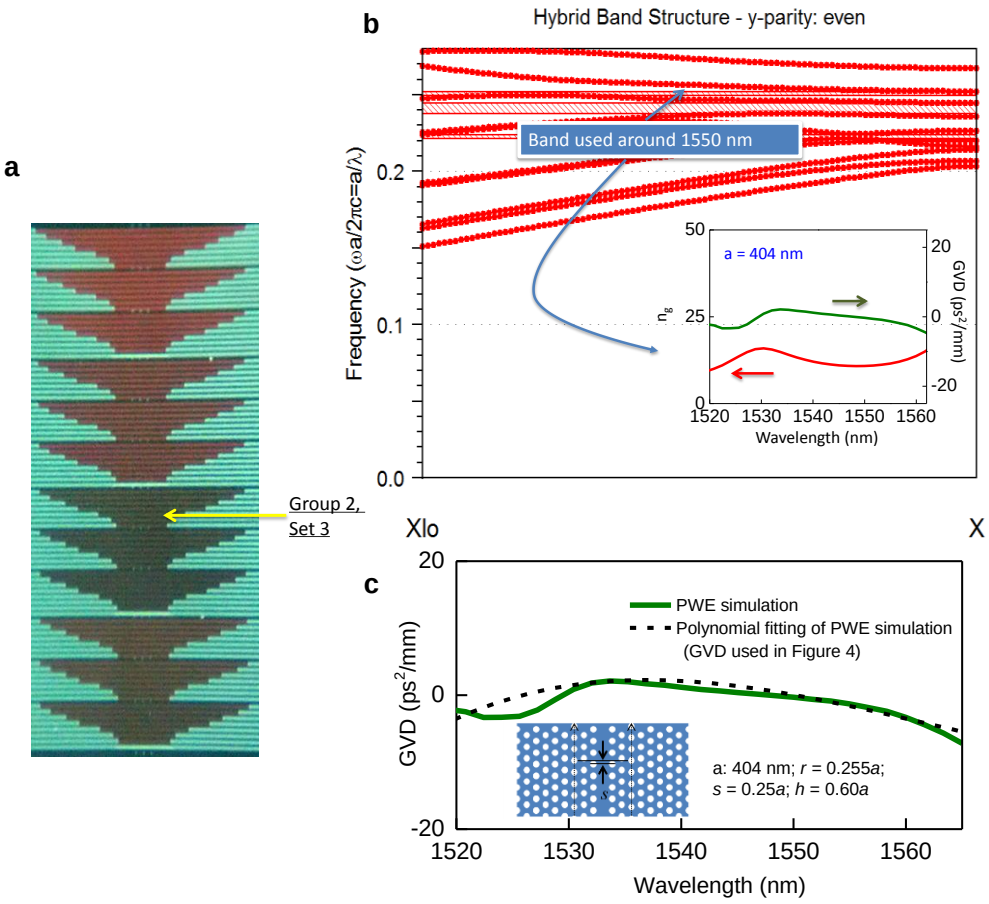

Figure S3 | Chip micrograph and GVD of the lattice-shifted low-GVD photonic crystal waveguide. a, Optical micrograph containing the low-GVD photonic crystal waveguides. **b**, Computed band structure of photonic crystal waveguide tested, through plane-wave expansion, in Figure 4 of the main text. The inset shows the corresponding group index and GVD curves resolved from the ninth band around 1550 nm, with lattice constant a = 404 nm. **c**, Comparison between the plane-wave-expansion-simulated GVD versus the fourth degree polynomial fitted GVD used in Figure 4 of the main text, with $\beta_2 = -3.5$ ps^2/mm, $\beta_3 = 0.5$ ps^3/mm, $\beta_4 = -0.005$ ps^4/mm, and $\beta_5 = -0.0025$ ps^5/mm, centered at 1560 nm. Inset shows the schematic of symmetric third-row shift (s) of the air-holes and parameters used in plane-wave expansion calculation.

is observed that the increase of n_g as a function of wavelength is reduced within 1530 nm to 1545 nm, corresponding a low-GVD section therein and a zero crossing near 1545 nm [SR5]. To apply the simulated GVD curve in NLSE calculation, we conducted fourth-order polynomial fitting, with $\beta_2 = -3.5$ ps^2/mm, $\beta_3 = 0.5$ ps^3/mm, $\beta_4 = -0.005$ ps^4/mm, and $\beta_5 = -0.0025$ ps^5/mm, centered at 1560 nm. The comparison between simulated and polynomial fitted GVD are displayed in Figure S3c, exhibiting good consistency.

IV. Modulation instability under the influence of TPA free carrier dispersion:

The electron-hole Drude dynamics also has concurrent effects on the modulation instability and spectral broadening. Here we analytically derived the MI gain spectrum according to the NLSE model with the Drude free-carrier dynamics shown earlier in Eq. 2. Using linear stability analysis, we assume

$$E = \left[\sqrt{P} + a(z,t)\right] e^{i\left[\gamma_{eff} P - \frac{k_0 k_c \beta_{TPA} \tau_f}{2h\nu_0 A_0^2} P^2\right] z} \qquad (S12)$$

$$N_c = \frac{\beta_{TPA}\tau_f}{2h\nu_0 A_0^2} P^2 + b(z,t) \qquad (S13)$$

Here *a* and *b* are the perturbations. Here the implicit assumption is the absorption is not yet too strong such that we can assume the steady-state solution has constant amplitude along the propagation. This is a necessary approximation because no analytic steady-state solution exists if we consider all the dynamical absorptions. It is valid at the beginning of the propagation where the MI starts to grow. The linearized equations are:

$$i\frac{\partial a}{\partial z} - \frac{\beta_2}{2}\frac{\partial^2 a}{\partial t^2} + \gamma_{eff} P(a + a^*) - k_0 k_c \sqrt{P} b = 0 \qquad (S14)$$

$$\frac{\partial b}{\partial t} = \frac{\beta_{TPA} P^{3/2}}{h\nu_0 A_0^2}(a + a^*) - \frac{b}{\tau_f} \qquad (S15)$$

Now assume:

$$a(z,t) = a_1 e^{i(Kz - \Omega t)} + a_2 e^{-i(Kz - \Omega t)} \qquad (S16)$$

$$b(z,t) = b_0 e^{i(Kz - \Omega t)} + b_0^* e^{-i(Kz - \Omega t)} \qquad (S17)$$

Plugging into the linearized equations, and collecting terms containing $e^{i(Kz-\Omega t)}$ and $e^{-i(Kz-\Omega t)}$, then we have the following three equations:

$$b_0 = \frac{\beta_{TPA} P^{3/2}}{h\nu_0 A_0^2 \left(\frac{1}{\tau_f} - i\Omega\right)}(a_1 + a_2^*) \qquad (S18)$$

$$0 = -Ka_1 + \frac{\beta_2 \Omega^2}{2} a_1 + \gamma_{eff} P a_1 + \gamma_{eff} P a_2^* - k_0 k_c \sqrt{P} b_0 \qquad (S19)$$

$$0 = Ka_2 + \frac{\beta_2 \Omega^2}{2} a_2 + \gamma_{eff} P a_2 + \gamma_{eff} P a_1^* - k_0 k_c \sqrt{P} b_0 \qquad (S20)$$

Replacing b_0 by a_1 and a_2*, we get two equations:

$$\begin{bmatrix} M_{11} & M_{12} \\ M_{21} & M_{22} \end{bmatrix} \begin{pmatrix} a_1 \\ a_2^* \end{pmatrix} = 0 \qquad (S21)$$

where: $M_{11} = -K + \frac{\beta_2\Omega^2}{2} + \gamma_0 P - \frac{k_0 k_c \beta_{TPA} P^2}{h\nu_0 A_0^2\left(\frac{1}{\tau_f} - i\Omega\right)}$, $M_{12} = M_{21} = \gamma_0 P - \frac{k_0 k_c \beta_{TPA} P^2}{h\nu_0 A_0^2\left(\frac{1}{\tau_f} - i\Omega\right)}$, $M_{22} = K + \frac{\beta_2\Omega^2}{2} + \gamma_0 P - \frac{k_0 k_c \beta_{TPA} P^2}{h\nu_0 A_0^2\left(\frac{1}{\tau_f} - i\Omega\right)}$. Nontrivial solution exists only if $M_{11}M_{22} - M_{12}M_{21} = 0$, then we have:

$$K = \pm\left|\frac{\beta_2\Omega}{2}\right|\sqrt{\Omega^2 + \frac{4\gamma_{eff}P}{\beta_2} - \frac{4k_0 k_c \beta_{TPA} P^2}{h\nu_0 A_0^2 \beta_2\left(\frac{1}{\tau_f} - i\Omega\right)}} \quad . \qquad (S22)$$

The resulting MI gain is found from 2·Im{K} and shown in Figure 6 of the main text. Figure S4 compares the MI gain spectra with and without the Drude FCD effect, calculated using Eq. S22. It is seen that, different from conventional Kerr MI utilized in optical parametric oscillators, MI gain is always guaranteed by Drude FCD regardless of MI frequency and present in both normal and anomalous group velocity dispersion.

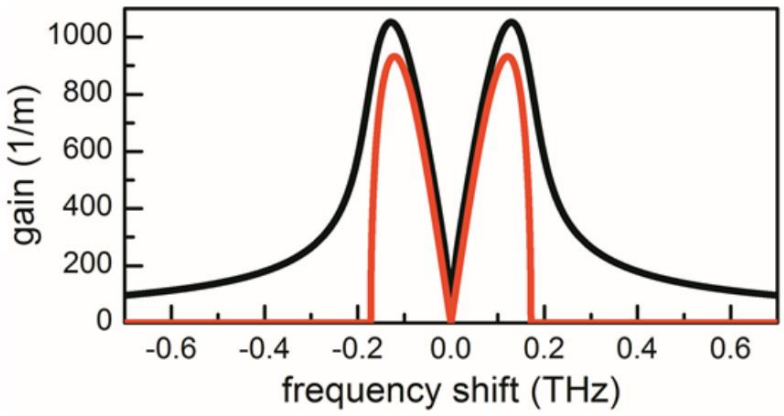

Figure S4 | Comparison of MI gain spectra analytically calculated with (black) and without (red) the Drude FCD effect. While the canonical Kerr MI has an apparent pump threshold, the FCD-perturbed MI features a thresholdless amplification and a broader gain bandwidth.

Supplementary References:

[SR1] G. P. Agrawal, *Nonlinear Fiber Optics, Third Edition* , Academic Press San Diego, 2001.

[SR2] M. F. Saleh, W. Chang, P. Hoelzer, A. Nazarkin, J. C. Travers, N. Y. Joly, P. St. J. Russell, and F. Biancalana, Theory of photoionization-induced blueshift of ultrashort solitons in gas-filled hollow-core photonic crystal fibers. *Phys. Rev. Lett.* **107**, 203902 (2011).

[SR3] C. Husko, P. Colman, S. Combrié, A. De Rossi, and C. W. Wong, Effect of multiphoton

absorption and free carriers in slow-light photonic crystal waveguides, *Opt. Lett.* **36**, 2239 (2011).

[SR4] L. Yin, Q. Lin, and G. P. Agrawal, Dispersion tailoring and soliton propagation in silicon waveguides. *Opt. Lett.* **31**, 1295 (2006).

[SR5] Y. Hamachi, S. Kubo, and T. Baba, Slow light with low dispersion and nonlinear enhancement in a lattice-shifted photonic crystal waveguide, *Opt. Lett.* **34**, 1072 (2009).

[SR6] S. A. Schulz, L. O'Faolain, D. M. Beggs, T. P. White, A. Melloni and T. F. Krauss, Dispersion engineered slow light inphotonic crystals: a comparison. *Journal of Optics* **12**, 101004 (2010).

[SR7] P. Colman, S. Combrié, G. Lehoucq, and A. De Rossi, Control of dispersion in photonic crystal waveguides using group symmetry theory, *Opt. Exp.* **20**, 13108 (2012).